Shear response of Fe-bearing $MgSiO_3$ post-perovskite at lower mantle pressures

By Arnaud METSUE[*1] and Taku TSUCHIYA[*1,†]

(Communicated by Ikuo KUSHIRO, M.J.A.)

Abstract: We investigate the shear response of possible slip systems activated in pure and Fe-bearing $MgSiO_3$ post-perovskite (PPv) through *ab initio* generalized stacking fault (GSF) energy calculations. Here we show that the [100](001) slip system has the easiest response to plastic shear among ten possible slip systems investigated. Incorporation of Fe^{2+} decreases the strength of all slip systems but does not change the plastic anisotropy style. Therefore, pure and Fe-bearing $MgSiO_3$ PPv should demonstrate similar LPO patterns with a strong signature of the [100](001) slip system. An aggregate with this deformation texture is expected to produce a $V_{SH} > V_{SV}$ type polarization anisotropy, being consistent with seismological observations.

Keywords: *ab initio* density functional computation, generalized stacking fault theory, seismic anisotropy, earth's D'' layer, post-perovskite

Introduction

Over the last thirty years, the lowermost part of the Earth's mantle, the D'' layer, has been recognized as being a seismological anisotropic structure, whereas the rest of the lower mantle is nearly isotropic.[1)–5)] Several observations suggest that the horizontally polarized shear wave (V_{SH}) is faster than the vertically polarized shear wave (V_{SV}) in most areas of the D'' layer,[3),4)] except beneath the Africa and Pacific low-velocity provinces.[2),5)] Several scenarios have been proposed for the splitting mechanism of the polarized shear waves in the D'' layer. One is the formation of shape-preferred orientations due to the alignment of fluid-inclusion[6)] or anisotropic atomic diffusion.[7)] Another more efficient origin can be found in the development of the lattice-preferred orientation (LPO) of $(Mg,Fe)SiO_3$ post-perovskite (hereafter PPv), which is thought to be the most abundant mineral in the D'' layer[8),9)] with a strong elastic anisotropy,[10)] during plastic deformation with anisotropic shear response of the slip systems, such as dislocation creep or mechanical twinning.[6)] Although several high-pressure experiments have therefore been performed to understand the plastic deformation mechanism of PPv,[11)–15)] results are still largely controversial primarily due to experimental technical difficulty as the (010) plane[11)] and the (001) plane[12)] for the stable slip plane. Most of these deformation experiments were conducted at room temperature, which is far low from the geophysically relevant temperature of the D'' region of $\sim$2500 K.[16),17)] However, a high-temperature deformation experiment[15)] also shows the (001) plane as the stable slip plane of PPv. This slip mechanism can explain the observed polarization anisotropy in the D'' layer.[10)]

Understanding and modelling the plastic deformation mechanisms require the knowledge of the resistance of all individual slip systems of PPv involved in the deformation mechanisms. For these purpose, theoretical and computation approaches are also of substantial importance. However, some theoretical studies have also suggested contradictive results as the (100) or (110) slip planes[18)] and (010)[19)] for PPv, primarily because these examined only particular structure modifications or calculated the generalized stacking fault (GSF) energies of limited slip planes. Also the calculations were conducted only for pure $MgSiO_3$ and the effect of Fe is still largely unclear. Another work of $MgGeO_3$ PPv, on the other hand, calculated the GSF of several slip systems[20)] and found that differences in ideal shear stress

[*1] Geodynamics Research Center, Ehime University, Ehime, Japan.
[†] Correspondence should be addressed: T. Tsuchiya, Geodynamics Research Center, Ehime University, 2-5 Bunkyo-cho, Matsuyama, Ehime 790-8577, Japan (e-mail: takut@sci.ehime-u.ac.jp).

doi: 10.2183/pjab.89.51

are very small for the [100](010), [100](011), and [100](001) systems. This suggests that these slip systems are almost equally likely, but the calculations were carried out at the pressure far higher than the PPv transition pressure of $MgGeO_3$. In this study, the GSF energies for the possible activated slip systems in pure and Fe-bearing $MgSiO_3$ PPv are calculated comprehensively at 120 GPa by means of the density functional computation method.

The GSF energy calculations, initiated by Vitek,[21] provide information on the ability of a crystal to be sheared homogeneously in a ⟨uvw⟩{hkl} slip system. This technique was applied to pure $MgSiO_3$ perovskite (Pv) and PPv[19] but have not been extended to more realistic mantle compositions, including Fe, so far. We considered ten possible slip systems for PPv, since the stable slip systems are not well constrained for this phase. These likely slip systems were modelled based on the following general criteria. The shear vectors, or Burgers vectors, were chosen from the shortest lattice vectors in order to minimize the elastic energy of the dislocation associated with the slip system, which is proportional to the square of the Burgers vector, the so-called Frank criteria.[22] For a given Burgers vector, the glide planes correspond to the largest d_{hkl} distance, i.e., to the lower Miller index of the {hkl} plane.[23] According to these criteria, ten possible slip systems emerged for the PPv phase: [100](010), [100](001), [100]{011}, [010](100), [010](001), [001](100), [001](010), [001]{110}, 1/2⟨110⟩(001), and 1/2⟨110⟩{110}. In order to investigate the effects of Fe on the response of the PPv to plastic shear, we substituted one atom of Mg close to the glide plane with ferrous Fe. The total energy of the Fe-bearing cell with a geophysically relevant iron concentration of 8.3%[24] was calculated within the internally consistent LDA+U formalism.[25] To examine the influence of the spin state on the shear response, Fe was treated both in the high spin (HS) and low spin (LS) states, even though several studies have suggested that Fe^{2+} remains in the HS state in the whole pressure range of the D'' layer.[25),26]

Calculation conditions

The value of the GSF energy was obtained by shearing half of a perfect crystal over the other half along the Burgers vector in a slip plane. A supercell was built by repeating the conventional orthorhombic structure of PPv (space group *Cmcm*, $Z = 4$)[8] three times perpendicularly to the slip plane. We checked that this supercell size assures the convergence of the calculations. A vacuum buffer of 4 Å was added at the top of the supercell to isolate the created defect. We found that this size of vacuum is sufficient to remove significant inter-layer interaction. The GSF energy was calculated at every 5% of shear along the Burgers vector and the results were fitted with a Fourier series, similarly to the previous studies.[19),20] These calculations were performed within the density functional theory[27] implemented in Quantum Espresso.[28] For the calculation of the Fe-bearing system, we adopted the internally consistent LSDA+U formalism,[29),30] where the on-site Coulomb interaction between the *d*-states of Fe was determined at 120 GPa in our previous study,[25] equal to 3.639 eV and to 5.408 eV for HS and LS, respectively. We applied the planewave method combined with *ab initio* psuedopotentials which are the same as those used in our previous studies.[8),10),25] The planewave cut-off energy was set to 70 Ry and the Brillouin zone was sampled on a grid built for each supercell geometry.

Generalized stacking fault energy

The GSF energies calculated for the [001](010), [100](001), and [010](100) slip systems are shown in Fig. 1 as well as for the seven other slip systems in Appendix. Three different shapes of GSF curves were found irrespective of the Fe incorporation: a single peak, a double peak, and a peak with shoulder(s). The glide along the [100] and 1/2⟨110⟩ directions is characterized by a single peak at 50% of shear. The GSF energy curves for the [001]{hk0} and [010](001) slip systems exhibit a local minimum for 50% of shear along the Burgers vector, indicating the presence of a stable stacking fault bounded by two partial dislocations with 1/2[001] and 1/2[010] Burgers vectors. The dissociation of these dislocations into two partial dislocations in the PPv phase was previously reported from a Peierls-Nabarro modelling of dislocation cores.[19),20] Finally, the [010](100) slip system displayed unstable stacking faults at 25% and 75% of shear. The value of the maximum GSF energies and, if it exists, the stable stacking fault energy for all the slip systems are given in Table 1. The present results for pure PPv are in reasonable agreement with the values obtained within the generalized gradient approximation (GGA).[31] Small differences are however seen in some cases, since the previous calculations were conducted using supercells smaller than in the present study in most cases and also with applying the GGA, which is widely known to underestimate elasticity of silicates.

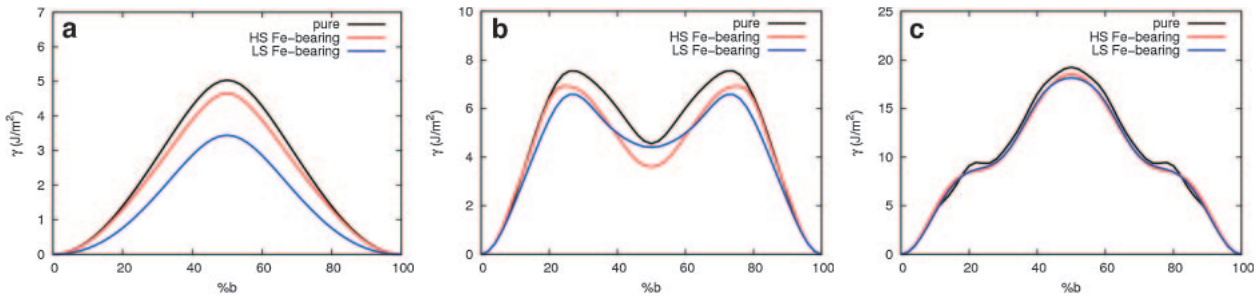

Fig. 1. Generalized stacking fault energy as a function of the shear for the [100](001) (a), [001](010) (b) and [010](100) (c) slip systems of pure and HS/LS Fe-bearing $MgSiO_3$ PPv.

The presence and the width of stable stacking faults in the structure offer an atomistic view of the deformation mechanisms. In particular, the extension of the dissociated dislocation structure affects the mobility of the defect.[23] We test the ability of the stacking fault to adsorb Fe by calculating the stable stacking fault energy variations by changing the distance between the single-point defect and the glide plane. Those from the glide planes for the [001]{hk0} and [010](001) slip systems are displayed in Fig. 2, indicating that Fe decreases the energy of the stable stacking fault when it is close to the glide plane, irrespective of the spin state. This demonstrates that Fe could be adsorbed in the slip plane, leading to a Cottrell atmosphere of Fe as reported in olivine,[32] which induces a longer faulted ribbon width proportional to the shear modulus and inversely proportional to the stacking fault energy,[23] for pure and Fe-bearing phases. In Fig. 2, larger reductions of the stacking fault energy are sometimes seen in the LS case than in the HS case, which implies that the deformation of PPv becomes relatively easier when iron is in the LS state. However, stability of iron spin state during gliding should be evaluated properly as shown in the following section.

To determine the width of the stacking fault, we apply the elastic theory of dislocations. A stacking fault is bounded by two partial dislocations with Burgers vectors of the partials b_p that are half of the total Burgers vector. The faulted ribbon width d is given by Ref. 23)

$$d = \frac{\mu_{[uvw]\{hkl\}}}{2\pi\gamma_{\text{stable}}} b_{p'}^2 \qquad [1]$$

where $\mu_{[uvw]\{hkl\}}$ is the orientation-dependent shear modulus of the slip system where the dislocations are dissociated. These shear moduli for pure and HS/LS Fe-bearing $MgSiO_3$ PPv given in Table 2 were calculated from the elastic constants calculated

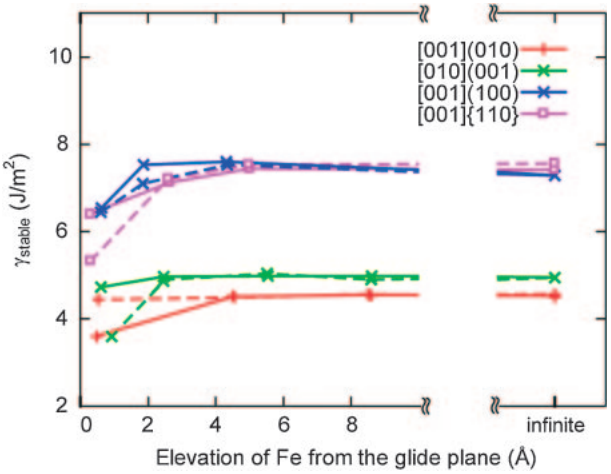

Fig. 2. Influence of the position of Fe on the stable stacking fault energies. γ_{stable} as a function of the elevation of the Fe atoms from the glide plane for the [001]{hk0} and [010](001) slip systems. Solid and dashed lines are the results for the HS and LS cases, respectively. The [100](001) system was found to give energies comparable to those of the [010](001) system.

from a previous study for the $MgSiO_3$ end-member phase[10] and for an $(Mg_{0.917}Fe_{0.083})SiO_3$ composition.[26] Table 1 clearly demonstrates the development of the Cottrell atmosphere with the adsorption of Fe. This tends to stabilize the extended dislocation configuration. Dislocation processes other than the glide for dissociated dislocations, for example cross-slip, might therefore be unfavourable.

Possible shear-induced spin transition in Fe-bearing $MgSiO_3$ PPv?

It is obvious from Fig. 1 that the incorporation of Fe in the PPv phase decreases the GSF energies of all slip systems. This means that Fe-bearing $MgSiO_3$ is sheared more easily than the pure phase. In addition, it seems that LS Fe decreases the GSF energies more compared to HS Fe, in particular for

Table 1. Characterization of the ten investigated slip systems at 120 GPa

Slip system	γ_{max} (J/m^2)	γ_{stable} (J/m^2)	d (Å)	ISS (GPa)
[100](010)	4.29			69.9
	6.01			78.1
	5.55*			71.7*
[100](001)	4.66			56.9
	5.04			63.4
	4.86*			61.8*
[100]{011}	5.75			72.6
	6.31			80.1
	4.91*			61.7*
[010](100)	18.53			82.5
	19.25			82.4
	21.02*			115.8*
[010](001)	15.63	4.72	24.37	109.1
	17.79	5.04	23.03	117.3
	18.11*	4.89*		131.2*
[001](100)	10.57	6.59	6.16	117.1
	11.35	7.35	5.62	119.0
	11.66*	9.01*		107.1*
[001](010)	6.93	3.60	12.31	69.4
	7.49	4.56	9.61	71.4
	7.50*	4.95*		78.0*
[001]{110}	10.09	6.39	6.40	103.6
	11.54	7.42	5.58	120.6
	11.42*	10.14*		101.6*
1/2⟨110⟩(001)	13.44			102.2
	15.81			120.1
	16.23*			120.0*
1/2⟨110⟩{110}	13.54			88.09
	13.65			100.04
	14.44*			133.4*

γ_{max} represents maximum of the GSF curve, γ_{stable} energy of the stable stacking fault, d the corresponding extension width, and ISS the ideal shear stress. The values for HS Fe-bearing and pure $MgSiO_3$ PPv are listed in the first and second lines, respectively. Values with * are earlier results for pure PPv obtained with the GGA.[31)]

Table 2. Orientation-dependent shear moduli of pure and HS/LS Fe-bearing $MgSiO_3$ PPv

	$MgSiO_3$	HS $(Mg_{0.917}Fe_{0.083})SiO_3$	LS $(Mg_{0.917}Fe_{0.083})SiO_3$
[100](010)	439	432	451
[100](001)	278	273	266
[100]{011}	336	330	333
[010](100)	295	298	303
[010](001)	439	432	451
[001](100)	278	273	266
[001](010)	295	298	303
[001]{110}	279	275	269
1/2⟨110⟩(001)	426	419	436
1/2⟨110⟩{110}	412	404	417

Values are calculated at 120 GPa from the elastic constants[10),26)] for the ten investigated slip system. The unit is GPa.

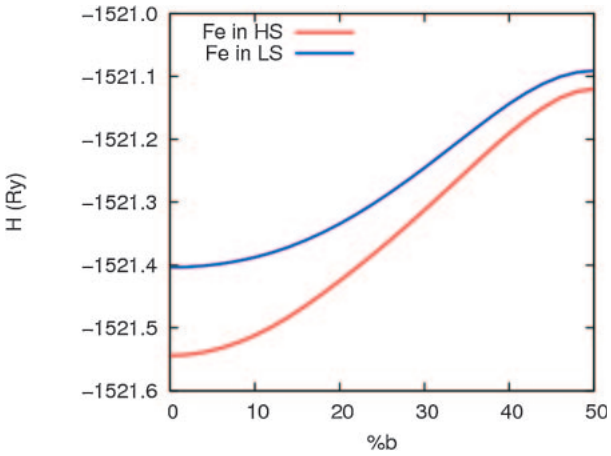

Fig. 3. Enthalpy variation of HS/LS $(Mg_{0.917}Fe_{0.083})SiO_3$ PPv as a function of shear along the [100] direction in the (001) slip plane.

the [100](001) slip system, because the stable atomic position of LS Fe is displaced along the [001] axis.[25),33)] The spin state of Fe is sensitive to the crystal field, which depends not only on the size of the site but also on the shape of the site.[34)] They can be affected by shear deformation. Therefore, we investigated a possible spin crossover induced by a shearing mechanism. We calculate the enthalpy of the HS and LS Fe-bearing $MgSiO_3$ PPv sheared along the [100] direction in the (001) slip plane. The enthalpy of a crystal with shear f[23)] is given by

$$H(P, f) = H(P, f = 0) + \gamma(f)S. \quad [2]$$

As shown in Fig. 3, the enthalpy difference between HS and LS decreases with increasing the value of the shear but the enthalpy of the HS Fe-bearing phase remains lower than the enthalpy of the LS Fe-bearing phase. Therefore, the shear mechanism is unlikely to induce a spin transition in $(Mg_{0.917}Fe_{0.083})SiO_3$ PPv in the D'' layer pressure range.

Ideal shear stress

To quantify the effects of Fe on the ease of shearing compared to the pure phase, we evaluate the ideal shear stress (ISS), the upper stress limit that a perfect crystal can suffer from plastic shear,[35] for pure and HS Fe-bearing phases. The ISS is the absolute maximum of the derivative of the GSF energy relative to the shear and the values for all investigated slip systems are given in Table 1. The values for pure $MgSiO_3$ PPv are consistent with the previous study.[19] The ISS decreases with the incorporation of Fe for all the slip systems, implying an intrinsic weakening of Fe-bearing PPv compared to the pure phase. This behaviour is similar to that observed in (Mg,Fe)SiO_3 Pv, where the incorporated Fe decreases the mechanical strength of the phase.[36] The Fe-induced weakening of the PPv phase might decrease the viscosity in the D'' layer and thus enhance the heat transport and mantle mixing.[37] Plastic anisotropy which results in the development of LPO can be analysed from the ISS.[23] The calculations of the ISS indicate that the [100](001) slip system has the lowest value both in the pure and Fe-bearing phases and might therefore be the dominant contribution to the development of the deformation textures of the PPv phase.

This is consistent with previous experimental results by Refs. 12) and 13) but different from those reported by Ref. 11) where the (100) and {110} slip planes were suggested to participate mainly to the deformation textures. However, the LPO texture dominated by the (100) plane reported could have been produced by the phase transformation process to PPv from $(Mg_{0.9}Fe_{0.1})SiO_3$ enstatite.[13),14] The previous theoretical studies[19),20] based on one-dimensional Peierls-Nabarro modelling suggest that the textures are dominated by the [001](010) slip system. However, the formulation of the Peierls-Nabarro model used in these studies cannot take into account possible three-dimensional spreading of the [001] dislocation which hardens the slip system.

Plastic anisotropy

Next, the degree of plastic anisotropy of the single crystal is addressed based on the Schmid law,[38] which links the critical resolved shear stress to the orientation and the value of an applied stress for every slip system. For a given orientation of the applied stress, we calculated the product of the ISS, assimilating to the critical resolved shear stress, with the inverse of the Schmid factor for the ten

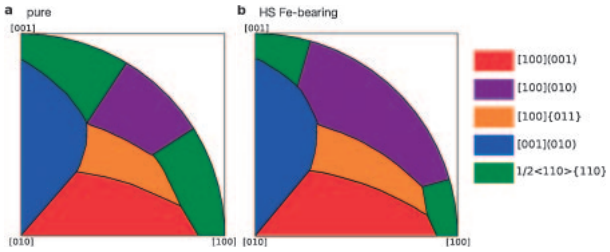

Fig. 4. Evaluation of the single-crystal plastic anisotropy of the PPv phase. Slip systems exhibiting the lowest applied critical stress depending on its orientation for single crystals of pure (a) and HS Fe-bearing PPv (b).

investigated slip systems. The critical applied stress to activate every slip system for all the orientation of the applied stress was then obtained. Figure 4 demonstrates the slip system associated with the lowest critical applied stress depending on the orientation of the applied stress for pure and HS Fe-bearing $MgSiO_3$ PPv. The same five slip systems exhibit low applied critical stress in the pure and Fe-bearing phases depending on the orientation of the applied stress, except a small difference between the domains of activation of the $1/2\langle 110\rangle\{110\}$ and [100](010) slip systems. The similar patterns indicate that the pure and Fe-bearing phases have the same plastic anisotropy style. Therefore, the pure and Fe-bearing phases should have similar polycrystalline deformation textures with a strong signature of the [100](001) slip system.

Discussion and conclusions

Other high-temperature deformation processes, for example dislocation climb or Coble creep, can be affected by the incorporation of Fe. Investigations on these thermally activated mechanisms at the D'' temperatures of $\sim$2500 K[16),17] should also be important. They however either strengthen or weaken the deformation texture but have no direct contribution to the preferred orientation style. Also, in terms of the homologous temperature, it is so far unclear that such temperatures are really high for the deformation of PPv at pressures over 120 GPa. In this condition, even the fundamental mechanical properties of iron-bearing PPv, including the ideal shear response, are still largely unclear, and thus they should have large implications. The present results predicting the [100](001) slip system for iron-bearing PPv agree well with the latest high-pressure deformation experiments suggesting the (001) slip plane both at room temperature[12] and at high mantle temperature.[15] In addition, LPO dominated by the (001) slip plane

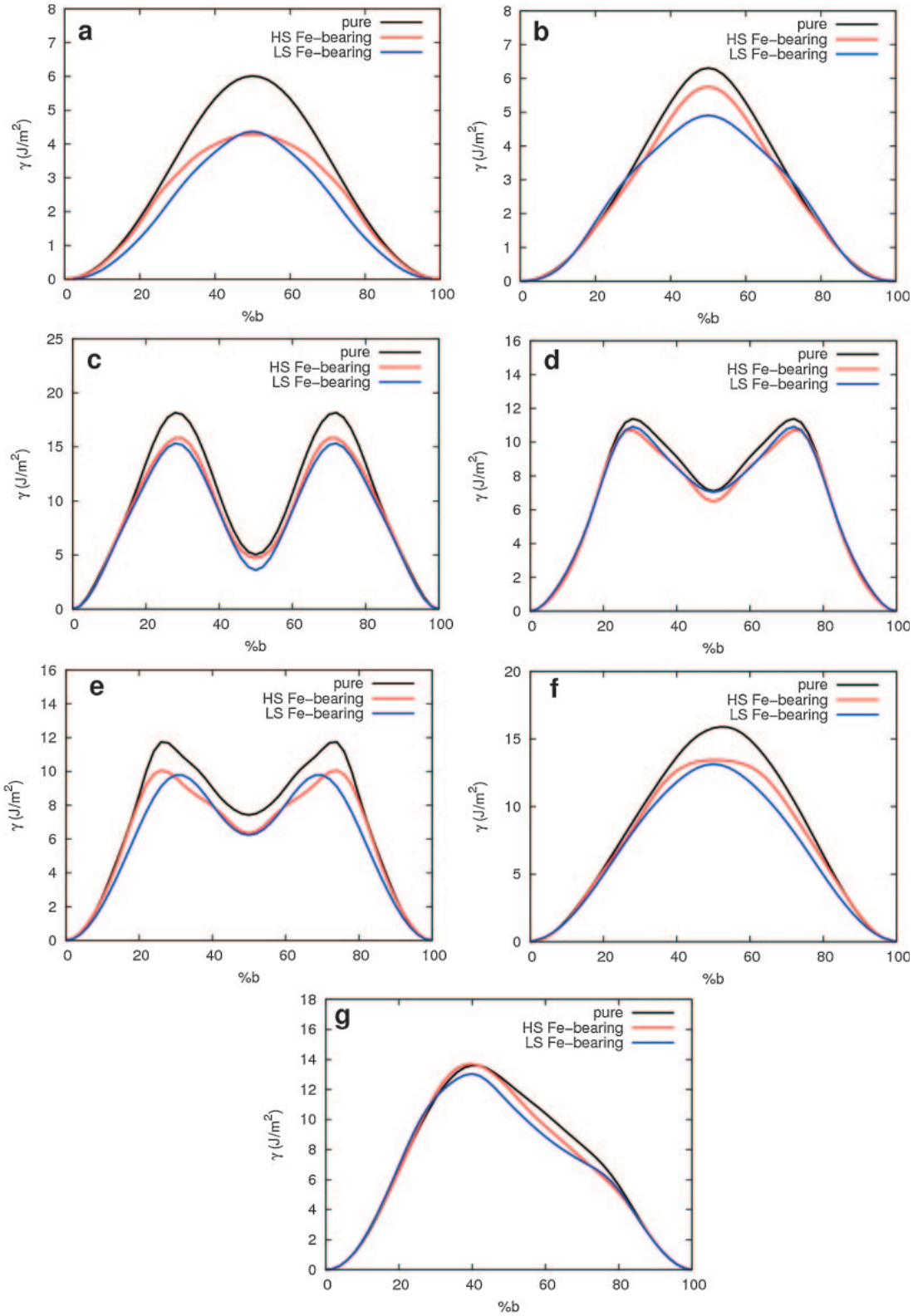

Fig. A1. Generalized stacking fault energies for the [100](010) (a), [100](011) (b), [010](001) (c), [001](100) (d), [001](110) (e), 1/2[110](001) (f), and 1/2[110](110) (g) calculated at 120 GPa.

leads to producing a $V_{SH} > V_{SV}$ type seismic shear wave splitting by several %,[10] being consistent with seismological observations.[3),39] It is therefore strongly suggested that the texture developed in PPv by plastic shear deformation can be responsible for the seismic anisotropy observed in the D'' layer.[1)–4)]

Acknowledgments

We thank S. Whitaker for helpful supports. This work is funded by the Global Center of Excellence program "Deep Earth Mineralogy" and KAKENHI 20001005 and 21740379.

Appendix: Generalized stacking fault energies for seven additional slip systems

Generalized stacking fault energies for the slip systems [100](010), [100](011), [010](001), [001](100), [001](110), 1/2[110](001), and 1/2[110](110) are shown in Fig. A1 in addition to those for three representative cases demonstrated in Fig. 1 in the main text.

References

1) Mitchell, B.J. and Helmberger, D.V. (1973) Shear velocities at the base of the mantle from observations of S and ScS. J. Geophys. Res. **78**, 6009–6020.
2) Panning, M. and Romanowicz, B. (2004) Inference on flow at the base of Earth's mantle based on seismic anisotropy. Science **303**, 351–353.
3) Kendall, J.-M. and Silver, P.G. (1996) Constraints from seismic anisotropy on the nature of the lowermost mantle. Nature **381**, 409–412.
4) Vinnik, L., Breger, L. and Romanowicz, B. (1998) Anisotropic structures at the base of the Earth's mantle. Nature **393**, 564–567.
5) Kawai, K. and Geller, R.J. (2010) The vertical flow in the lowermost mantle beneath the Pacific from inversion of seismic waveforms for anisotropic structure. Earth Planet. Sci. Lett. **297**, 190–198.
6) Mainprice, D., Barruol, G. and Ismail, W. (2000) From single crystal to polycrystal. *In* Eath's Deep Interior: Mineral Physics and Tomography from the Atomic to the Global Scale, AGU monograph (eds. Karato, S.-I., Forte, A.M., Liebermann, R.C., Masters, G., and Stixrude, L., Am. Geophys. Union), Vol. 117, pp. 237–264.
7) Ammann, M.W., Brodholt, J.P., Wookey, J. and Dobson, D.P. (2010) First-principles constraints on diffusion in lower-mantle minerals and a weak D'' layer. Nature **465**, 462–465.
8) Tsuchiya, T., Tsuchiya, J., Umemoto, K. and Wentzcovitch, R.M. (2004) Phase transition in $MgSiO_3$ perovskite in the Earth's lower mantle. Earth Planet. Sci. Lett. **224**, 241–248.
9) Murakami, M., Hirose, K., Kawamura, K., Sata, N. and Ohishi, Y. (2004) Post-perovskite phase transition in $MgSiO_3$. Science **304**, 855–858.
10) Tsuchiya, T., Tsuchiya, J., Umemoto, K. and Wentzcovitch, R.M. (2004) Elasticity of post-perovskite $MgSiO_3$. Geophys. Res. Lett. **31**, L14603.
11) Merkel, S., McNamara, A.K., Kubo, A., Speziale, S., Miyagi, L., Meng, Y., Duffy, T.S. and Wenk, H.-R. (2007) Deformation of (Mg,Fe)SiO_3 post-perovskite and D'' anisotropy. Science **316**, 1729–1732.
12) Miyagi, L., Kanitpanyacharoen, W., Kaercher, P., Lee, K. and Wenk, H. (2010) Slip systems in $MgSiO_3$ post-perovskite: implications for D'' anisotropy. Science **329**, 1639–1641.
13) Miyagi, L., Kanitpanyacharoen, W., Stackhouse, S., Militzer, B. and Wenk, H. (2011) The enigma of post-perovskite anisotropy: deformation versus transformation textures. Phys. Chem. Minerals **38**, 665–678.
14) Okada, T., Yagi, T., Niwa, K. and Kikegawa, T. (2010) Lattice-preferred orientations in post-perovskite-type $MgGeO_3$ formed by transformations from different pre-phases. Phys. Earth Planet. Int. **180**, 195–202.
15) Hirose, K., Nagaya, Y., Merkel, S. and Ohishi, Y. (2010) Deformation of $MnGeO_3$ post-perovskite at lower mantle pressure and temperature. Geophys. Res. Lett. **37**, L20302.
16) Brown, J.M. and Shankland, T.J. (1981) Thermodynamic properties in the Earth as determined from seismic profiles. Geophys. J. R. astr. Soc. **66**, 579–596.
17) Kawai, K. and Tsuchiya, T. (2009) Temperature profile in the lowermost mantle from seismological and mineral physics joint modeling. Proc. Natl. Acad. Sci. U.S.A. **106**, 22119–22123.
18) Oganov, A.R., Martonak, R., Laio, A., Raiteri, P. and Parrinello, M. (2005) Anisotropy of Earth's D'' layer and stacking faults in the $MgSiO_3$ post-perovskite phase. Nature **438**, 1142–1144.
19) Carrez, P., Ferré, D. and Cordier, P. (2007) Implications for plastic flow in the deep mantle from modelling dislocations in $MgSiO_3$ minerals. Nature **446**, 68–70.
20) Metsue, A., Carrez, P., Mainprice, D. and Cordier, P. (2009) Numerical modelling of dislocations and deformation mechanisms in $CaIrO_3$ and $MgGeO_3$ post-perovskites—Comparison with $MgSiO_3$ post-perovskite. Phys. Earth Planet. Int. **174**, 165–173.
21) Vitek, V. (1968) Intrinsic stacking faults in body-centered cubic crystals. Phil. Mag. **18**, 773–786.
22) Cordier, P. (2002) Dislocations and slip systems of mantle minerals. *In* Reviews in Mineralogy and Geochemistry (eds. Karato, S.-I. and Wenk, H.-R., Min. Soc. Am.), Vol. 51, pp. 137–180.
23) Hirth, J.P. and Lothe, J. (1982) Theory of Dislocations. Wiley, New York.
24) Kesson, S.E., Fitz Gerald, J.D. and Shelley, J.M. (1998) Mineralogy and dynamics of a pyrolite lower mantle. Nature **393**, 252–255.
25) Metsue, A. and Tsuchiya, T. (2011) Lattice dynamics and thermodynamic properties of (Mg,Fe^{2+})-SiO_3 postperovskite. J. Geophys. Res. **116**,

B08207.
26) Stackhouse, S., Brodholt, J.P., Dobson, D.P. and Price, D.G. (2006) Electronic spin transitions and the seismic properties of ferrous iron-bearing $MgSiO_3$ post-perovskite. Geophys. Res. Lett. **33**, L12S03.
27) Hohenberg, P. and Kohn, W. (1964) Inhomogeneous Electron Gas. Phys. Rev. **136**, B864–B871.
28) Giannozzi, P., Baroni, S., Bonini, N., Calandra, M., Car, R., Cavazzoni, C., Ceresoli, D., Chiarotti, G.L., Cococcioni, M., Dabo, I., Corso, A.D., de Gironcoli, S., Fabris, S., Fratesi, G., Gebauer, R., Gerstmann, U., Gougoussis, C., Kokalj, A., Lazzeri, M., Martin-Samos, L., Marzari, N., Mauri, F., Mazzarello, R., Paolini, S., Pasquarello, A., Paulatto, L., Sbraccia, C., Scandolo, S., Sclauzero, G., Seitsonen, A.P., Smogunov, A., Umari, P. and Wentzcovitch, R.M. (2009) QUANTUM ESPRESSO: a modular and open-source software project for quantum simulations of materials. J. Phys. Condens. Matter **21**, 395502–395521.
29) Cococcioni, M. and de Gironcoli, S. (2005) Linear response approach to the calculation of the effective interaction parameters in the LDA+U method. Phys. Rev. B **71**, 035105.
30) Tsuchiya, T., Wentzcovitch, R.M., da Silva, C.R.S. and de Gironcoli, S. (2006) Spin transition in magnesiowüstite in Earth's lower mantle. Phys. Rev. Lett. **96**, 198501.
31) Carrez, P., Ferre, D. and Cordier, P. (2007) Peierls-Nabbaro model for dislocations in $MgSiO_3$ post-perovskite calculated at 120 GPa from first principles. Phil. Mag. **87**, 3229–3247.
32) Ando, J., Shibata, Y., Okajima, Y., Kanagawa, K., Furusho, M. and Tomioka, N. (2001) Striped iron zoning of olivine induced by dislocation creep in deformed peridotites. Nature **414**, 893–895.
33) Umemoto, K., Wentzcovitch, R.M., Yu, Y.G. and Requist, R. (2008) Spin transition in $(Mg,Fe)SiO_3$ perovskite under pressure. Earth Planet. Sci. Lett. **276**, 198–206.
34) Burns, R. (1970) Mineralogical Applications of Crystal Field Theory. Cambridge University Press, London.
35) Paxton, A.T., Gumbsch, P. and Methfessel, M. (1991) A quantum mechanical calculation of the theoretical strength of metals. Philos. Mag. Lett. **63**, 267–274.
36) Chen, J., Girard, J., Couvy, H., Weidner, D. and Wang, Y. (2010) Influence of iron on the strength of silicate perovskite at high pressure. Eos Trans. AGU **91**, West. Pac. Geophys. Meet. Suppl., Abstract V21A–098.
37) Samuel, H. and Tosi, N. (2012) The influence of post-perovskite strength on the Earth's mantle thermal and chemical evolution. Earth Planet. Sci. Lett. **323–324**, 50–59.
38) Schmid, E. and Boas, W. (1950) Plasticity of Crystals. F.A. Hughes & Co. limited, London.
39) Wenk, H., Cottaar, S., Tomé, C., McNamara, A. and Romanowicz, B. (2011) Deformation in the lowermost mantle: From polycrystal plasticity to seismicanisotropy. Earth Planet. Sci. Lett. **306**, 33–45.

(Received Aug. 11, 2012; accepted Nov. 14, 2012)